



Phonon-assisted entanglement between two quantum dots coupled to a plasmonic nanocavity

M.A. Antón

Facultad de Óptica y Optometría, Universidad Complutense de Madrid, C/ Arcos de Jalón 118, 28037 Madrid, Spain

ARTICLE INFO

Keywords:

Entanglement
Plasmonic nanocavities
Phonon effects

ABSTRACT

We theoretically investigate the influence of a phonon bath on entangled generation between two semiconductor quantum dots coupled to a plasmonic nanocavity and coherently driven by an external optical field. Our study reveals that phonons could be useful in a certain range of system parameters where a subradiant state preparation is possible. We point out that this behavior is due to the fact that phonon environment modify the radiative properties of the two-qubit inducing different decay rates between the collective states of the system. The influence of the factors characteristic of quantum dot systems and plasmonic nanocavity such as energy mismatch in different dots, different plasmonic cavity losses as well as coupling to phonons is analyzed. The entanglement can be controlled via different external parameters such as the cavity detuning, the Rabi frequency of the driving field and the resonance frequency of the QDs.

1. Introduction

Quantum information processing is an active research field in which quantum entanglement of superposition states is the key to perform the primordial quantum operations [1–3]. Different systems have been proposed for entanglement such as photons [4,5], atoms and molecules [6] and solid state systems as cold ions [7–9], quantum dots (QDs) interacting with microcavities [10–14], and superconducting circuits [15, 16]. However, interaction of quantum systems with the environment may result in decoherence, thereby degrading the entanglement [17, 18]. Cavity quantum electrodynamics (cavity QED) has been used to manipulate and protect the entanglement of qubits from their environment [19,20], and prolong entangled time [21–24]. In this context, the integration of semiconductor QDs with (MNP) provides useful means to couple light and matter enabling strong confinement of light and thus increasing the light–matter interaction [25]. Thus, hybrid-plasmonic nanostructures, i.e. structures where excitons in QDs are coupled to localized surface plasmon (LSP) of a metal nanoparticle (MNP) at optical frequencies can be exploited as nanoscale cavities. Several studies have shown the modification of spontaneous emission [26] and resonance fluorescence of quantum emitters when placed near plasmonic nanostructures [27,28]. In particular, in recent years, the entanglement dynamics of qubits near plasmonic nanostructures have been investigated [29–31] proving that these dissipative plasmonic nanostructures can produce entanglement between QDs in a analogous way to previous proposals to entangle interacting atoms through common coupling to a lossy cavity [32]. Moreover longer entanglement distances can be achieved by utilizing one-dimensional wedge waveguides [33–35], and nanorings [36].

Despite their potential for displaying quantum plasmonics effects, previous predictions of plasmon-induced entanglement in QDs-MNP nanostructures have been limited to systems in which the contribution of electron–phonon is ignored. However, it has been pointed out that the decoherence effects induced by the solid state environment of QD excitons are dominated by interactions with longitudinal acoustic phonons via the deformation potential coupling [37]. For example, exciton–phonon interactions are known to have a significant effect on the neutral exciton photoluminescence [38,39] and in self-assembled quantum dots coupled to nanocavities [13,40–42]. For these reasons, phonon effects in hybrid plasmonic deserve to be considered.

It is interesting to note that although the interaction with phonon environment is usually considered as a source of decoherence, coupling with a dissipative environment can also generate entanglement [43–47]. In this sense, the study of the effect of phonons on the dynamics of a quantum dot has been the subject of considerable interest. Examples include the study of entanglement between two QDs [48,49], entanglement between two charge qubits induced by a common dissipative environment [50], and entanglement of a laser driven pair of two closely two-level qubits interacting via dipole–dipole [51], among others. Recently, phonons have been actively used in optical control schemes of QD states to prepare the exciton or biexciton state of the QD [52,53].

In view of this, the aim of this paper is to investigate the role of phonon-assisted transitions on entanglement between two QDs coupled to a plasmonic nanostructure. The main idea is to use phonon coupling as a low frequency reservoir which can change the radiative properties

E-mail address: antonm@ucm.es.

<https://doi.org/10.1016/j.optcom.2021.127811>

Received 16 July 2021; Received in revised form 19 November 2021; Accepted 13 December 2021

Available online 17 December 2021

0030-4018/© 2021 The Author(s). Published by Elsevier B.V. This is an open access article under the CC BY license (<http://creativecommons.org/licenses/by/4.0/>).

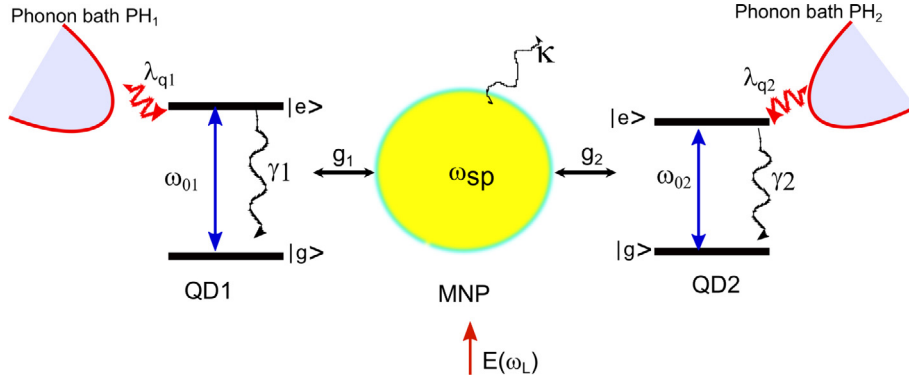


Fig. 1. Two QDs coupled to a MNP. The transition frequencies of the QDs are ω_{01} , ω_{02} , respectively. The MNP support longitudinal plasmons of frequency ω_{sp} . The QDs are coupled to independent phonon baths with exciton-phonon coupling constants λ_{qj} . Each QD decay to the vacuum with decay rate γ_j , and κ is the decay rate of the MNP. The hybrid system is driven by an external field of frequency ω_L .

of the quantum dots [12,54] and drive the qubits into a subradiant state. In particular, we will develop a theoretical model by coupling the qubits with the external field and the plasmonic cavity modes and including the interaction of each QD with two independent phonon baths. It is found that in certain conditions, the phonon environments can enhance the entanglement.

The paper is organized as follows: Section 2 establishes a model to describe the two-QDs interacting with a metallic nanoparticle taking into account the interaction between the QDs and the bosonic baths, and we derive an effective Hamiltonian which allows us to obtain the dynamical equations of the matrix density elements of the atomic system. In Section 3, we analyze the effect of the phonon interaction on entanglement of the two QDs. Finally, Section 4 summarizes the main conclusions.

2. Theoretical model

The system under study, displayed in Fig. 1, consists in two QDs placed in close proximity to a metal particle (MNP) of radius a on the nanometer scale. Each QD is modeled as a two-level system with ground state $|g\rangle$, and upper state $|e\rangle$. The transition frequency for each QD is $\omega_{0j} = \omega_{ej} - \omega_{gj}$, ($j = 1, 2$), and the transition electric dipole moment is $\vec{\mu}_{ge}$. The distances between the QDs and the center of the MNP are R_1 and R_2 , respectively. The system is driven by an external laser field of frequency ω_L and a slowly varying amplitude E_L , given by

$$\vec{E}_L(t) = \frac{1}{2} E_L (e^{-i\omega_L t} + e^{i\omega_L t}), \quad (1)$$

This oscillating electric field will generate plasmon oscillations in the MNP, and electric dipoles in the QD, which interact with each other via the dipole-dipole interaction (DDI). The optical response of the MNP can be described by its dielectric function $\epsilon_m(\omega)$ that we take in a renormalized Drude approximation [55],

$$\epsilon_m(\omega) = \epsilon_\infty - \frac{\omega_p^2}{\omega^2 + i\gamma_p\omega}, \quad (2)$$

where ϵ_∞ is the high-frequency limit of the metal dielectric function, ω_p is the bulk plasmon frequency, and γ_p is the Landau damping constant. The resonance frequency of the MNP ω_{sp} can be tuned by tailoring the radius of the MNP, which allows us to match the plasmonic resonance to a specific transition frequency of the QDs. The dielectric function of each QD is denoted as ϵ_s , while that of the host medium is denoted as ϵ_B . Furthermore, we assume that the two QDs are coupled with two independent phonon reservoirs PH_1 and PH_2 at temperatures T_1 and T_2 , respectively, as sketched in Fig. 1.

The two-level excitonic term of the Hamiltonian of the i th QD can be expressed as

$$H_0 = \frac{\hbar}{2} \sum_{j=1}^2 \omega_{0j} \sigma_z^{(j)} \quad (3)$$

where $\hbar\omega_{0j}$ is the excitonic energy of the QD and $\sigma_\pm^{(j)}$, $\sigma_z^{(j)}$ are the Pauli matrices acting in the space spanned by the states $|g\rangle$ and $|e\rangle$. Each QD interacts with its local phononic reservoir which are described as a set of harmonic oscillators with frequency ω_{qj} ($j=1,2$), respectively. The QD interaction-boson bath interaction is described with a spin-phonon Hamiltonian [45,56] given by

$$H_{ph} = \hbar \sum_{qj} \omega_{qj} b_{qj}^\dagger b_{qj} + \hbar \sum_{q1} \lambda_{q1} \sigma_z^{(1)} (b_{q1}^\dagger + b_{q1}) + \hbar \sum_{q2} \lambda_{q2} \sigma_z^{(2)} (b_{q2}^\dagger + b_{q2}). \quad (4)$$

where b_{qj}^\dagger (b_{qj}) is the creation(annihilation) phonon operator and λ_{qj} ($j = 1, 2$) is the coupling constant of the atomic-phonon bath interaction.

The interaction between the two QDs via electric dipole-dipole is given by

$$H_{D-D} = \hbar J_D (\sigma_+^{(1)} \sigma_-^{(2)} + \sigma_+^{(2)} \sigma_-^{(1)}), \quad (5)$$

where J_D is the coupling constants which is assumed to be given by $J_D = \frac{3}{4} \gamma \left[(1 - 3 \cos^2 \theta) \frac{\cos(kR)}{(kR)^3} \right]$, where θ is the angle between the transition dipole vector $\vec{\mu}_{ge}$ and the vector connecting the two qubits, i.e., \vec{R} , and γ_j is the single-qubit spontaneous decay rate.

The QDs excitons interact with a single plasmonic cavity mode of frequency ω_{sp} :

$$H_{p-c} = \hbar \omega_{sp} a^\dagger a, \quad (6)$$

where a (a^\dagger) is the annihilation(creation) operator for elementary plasmonic excitations with angular frequency ω_{sp} which satisfy bosonic commutation relations. The QDs interact with the plasmonic cavity mode via the coupling Hamiltonian

$$H_{e-p} = \hbar \omega_{sp} a^\dagger a + \hbar \sum_{j=1}^2 g_j (a^\dagger \sigma_j + a \sigma_j^\dagger), \quad (7)$$

with coupling constants g_j , ($j = 1, 2$) which are given by [57]

$$g_j = \frac{\mu_{eg}^{(j)}}{R_j^3} \sqrt{\frac{3\eta a^3}{4\pi\epsilon_0}}, \quad (8)$$

where $\eta = 1/\frac{d}{d\omega} \text{Re}[\epsilon_m(\omega)]_{\omega=\omega_{sp}}$.

Finally, the interaction between the external laser field and the QDs is given by

$$H_{ext} = \hbar \sum_{j=1}^2 \Omega_j \left(\sigma_+^j e^{-i\omega_L t} + \sigma_-^j e^{i\omega_L t} \right), \quad (9)$$

where $\Omega_j = \frac{|\mu_{ge}^j| E_L}{2\hbar}$ is the Rabi frequency of the optical field.

After performing a transformation to a frame rotating with the driving field frequency ω_L , the total Hamiltonian describing this system can be expressed as

$$H = \frac{\hbar}{2} \sum_{j=1}^2 \Delta_{Lj} \sigma_z^{(j)} + \hbar J_D \left(\sigma_+^{(1)} \sigma_-^{(2)} + \sigma_+^{(2)} \sigma_-^{(1)} \right) + \hbar \sum_{j=1}^2 \Omega_j \left(\sigma_+^j + \sigma_-^j \right) + \hbar \delta_c a^\dagger a + \hbar \sum_{j=1}^2 g_j \left(a^\dagger \sigma_j + a \sigma_j^\dagger \right) + H_{Ph}, \quad (10)$$

where $\Delta_{Lj} = (\omega_{0j} - \omega_L)$ ($j = 1, 2$) and $\delta_c = (\omega_L - \omega_{sp})$ are the detuning of the optical field with the transition frequency of each atom, and the frequency of the plasmonic cavity, respectively.

We describe the dynamics of the system by means of the master equation for the density matrix, ρ , including the effects of the environment via the phenomenological Lindblad terms [58]

$$\frac{\partial \rho}{\partial t} = -\frac{i}{\hbar} [H, \rho] + L_{QD} \rho + L_c \rho, \quad (11)$$

where L_{QD} accounts for dipole decay of the QD excitons, and L_c represents plasmonic cavity decay. These Liouvillian operators are defined as follows:

$$L_{QD} \rho = -\frac{1}{2} \sum_{i,j=1}^2 \gamma_{ij} \left[\sigma_+^{(j)} \sigma_-^{(i)} \rho - 2 \sigma_-^{(i)} \rho \sigma_+^{(j)} + \rho \sigma_+^{(j)} \sigma_-^{(i)} \right],$$

$$L_c \rho = -\frac{\kappa}{2} \left[a^\dagger \rho - 2 a \rho a^\dagger + \rho a^\dagger a \right], \quad (12)$$

where γ_{ij} ($i = j$) are the spontaneous emission rates of the quantum dots, whereas γ_{ij} ($i \neq j$) describe the collective damping, and κ represents the plasmonic cavity decay rate which is given by $\kappa = 2\eta \text{Im}[\epsilon_m(\omega)]_{\omega=\omega_{sp}}$ [57].

Now, we are interested in deriving an effective Hamiltonian for the atomic system by eliminating the field operators of the cavity mode in Eq. (10). This can be accomplished safely if the coupling constants and the decay rates are such that $\kappa \gg g_j \gg \gamma_j$. This condition is fully satisfied in the considered hybrid plasmonic system, since the dissipation rates in QDs are of the order on 0.1–1 GHz which are several orders of magnitude smaller than those associated with plasmonic nanoantennas (in the range of 100 THz) [59]. In order to eliminate the plasmonic cavity mode we apply an unitary transformation $U_1 = \exp(\beta_D)$, where

$$\beta_D = \sum_{j=1}^2 \left(\beta_j \sigma_+^{(j)} a - \beta_j^* a^\dagger \sigma_-^{(j)} \right), \quad (13)$$

β_j being

$$\beta_j = -i \frac{g_j}{\kappa/2 + i\delta_c}. \quad (14)$$

Using the Baker-Campbell- Hausdorff formula, the Hamiltonian H given in Eq. (10) transforms according to

$$H^{(1)} = e^{-\beta_D^\dagger} H e^{\beta_D} = \sum_{n=0}^{\infty} \frac{\beta_D^n}{n!} [\beta_D, H]_n \quad (15)$$

where $[A, B]_{n+1} = [A, [A, B]_n]$. Since in our system $\kappa \gg g_j$, then from Eq. (14) is evident that $|\beta_j| \ll 1$. This allows to conveniently truncate the transform at the third and higher terms of β_D . Taking into account the bath correlations

$$\langle a^\dagger(\omega') a(\omega) \rangle = 0, \quad (16)$$

$$\langle a(\omega') a^\dagger(\omega) \rangle = \delta(\omega' - \omega),$$

and tracing over the photon bath operators, we derive the master equation for the QDs:

$$\frac{\partial \rho^{(1)}}{\partial t} = -\frac{i}{\hbar} [H^{(1)}, \rho^{(1)}] + L_{QD}^{(1)} \rho^{(1)} + L_c^{(1)} \rho^{(1)}, \quad (17)$$

where the effective Hamiltonian reads

$$H^{(1)} = \frac{\hbar}{2} [(\Delta_0 + \Delta_L) \sigma_z^j] - \hbar \sum_{j=1}^2 \Omega_j \left(\sigma_-^j + \sigma_+^j \right) + \hbar J_{eff} \left(\sigma_+^{(1)} \sigma_-^{(2)} + \sigma_+^{(2)} \sigma_-^{(1)} \right) + H_{Ph}, \quad (18)$$

with

$$\Delta_0 = \omega_1 - \omega_2,$$

$$\Delta_L = \omega_2 - \omega_L - \frac{g_j^2 \delta_c}{\kappa^2/4 + \delta_c^2},$$

$$J_{eff} = J_D + \frac{g_1 g_2 \delta_c}{\kappa^2/4 + \delta_c^2}. \quad (19)$$

As follows from Eq. (19), the interaction with the plasmonic cavity modes shifts the transition frequency of the QDs, and modifies the dipole-dipole interaction J_D between the two qubits and, which is necessary for the generation of entanglement in this system. It is worth noting that the condition $\Delta_L = 0$ corresponds to quasi-resonance of the driving field with the second QD, and $\Delta_0 = 0$ means that the two QDs have the same transition frequency.

In addition, the unitary transformation $U^{(1)}$ induces new decay terms Γ_j^M , and Γ_{ij}^M that enhance the decay rate of the QDs, namely,

$$L_T^{(1)} \rho^{(1)} \equiv L_{QD}^{(1)} \rho^{(1)} + L_c^{(1)} \rho^{(1)}$$

$$= \frac{(\gamma_j + \Gamma_j^M)}{2} \sum_j \left[\sigma_+^{(j)} \sigma_-^{(j)} \rho^{(1)} - 2 \sigma_-^{(j)} \rho^{(1)} \sigma_+^{(j)} + \rho^{(1)} \sigma_+^{(j)} \sigma_-^{(j)} \right]$$

$$- \frac{\Gamma_{ij}^M}{2} \sum_{i \neq j} \left[\sigma_+^{(j)} \sigma_-^{(i)} \rho^{(1)} - 2 \sigma_-^{(i)} \rho^{(1)} \sigma_+^{(j)} + \rho^{(1)} \sigma_+^{(j)} \sigma_-^{(i)} \right], \quad (20)$$

with

$$\Gamma_j^M = \frac{\kappa_j |\beta_j|^2}{2} = \frac{\kappa_j}{2} \frac{g_j^2}{\kappa^2/4 + \delta_c^2},$$

$$\Gamma_{ij}^M = \gamma_{ij} + \frac{\kappa_j \beta_i \beta_j^*}{2}.$$

Before removing the phonon bath modes, it is very convenient to switch from the current basis given by $|gg\rangle$, $|ee\rangle$, $|ge\rangle$, $|eg\rangle$ to the Dicke basis, which can be derived from diagonalization of the part of the effective Hamiltonian, $H_D = \frac{\hbar}{2} [(\Delta_0 + \Delta_L) \sigma_z^{(1)} + \Delta_L \sigma_z^{(2)}] + \hbar (J_{eff} \sigma_+^{(1)} \sigma_-^{(2)} + J_{eff}^* \sigma_-^{(1)} \sigma_+^{(2)})$. The obtained eigenstates for the system are given by

$$|g\rangle = |gg\rangle,$$

$$|s\rangle = \beta |ge\rangle + \alpha |eg\rangle,$$

$$|a\rangle = \alpha |ge\rangle - \beta |eg\rangle,$$

$$|e\rangle = |ee\rangle, \quad (21)$$

with

$$\alpha = \frac{J_{eff}}{\sqrt{d^2 + J_{eff}^2}},$$

$$\beta = \frac{d}{\sqrt{d^2 + J_{eff}^2}},$$

$$d = \sqrt{\Delta_0^2/4 + J_{eff}^2} - \Delta_0/2. \quad (22)$$

The eigenvalues corresponding to the states are

$$\lambda_e = \frac{\Delta_0}{2} + \Delta_L,$$

$$\lambda_g = -\left(\frac{\Delta_0}{2} + \Delta_L \right),$$

$$\lambda_s = \frac{\Delta_0}{2} + \Delta_L + \sqrt{\left[\frac{\Delta_0}{2}\right]^2 + J_{eff}^2},$$

$$\lambda_a = \frac{\Delta_0}{2} + \Delta_L - \sqrt{\left[\frac{\Delta_0}{2}\right]^2 + J_{eff}^2}. \quad (23)$$

In order to express the Hamiltonian given in Eq. (18) in the new basis, we follow the procedure given in [60]. In brief, if we denote by λ_i the eigenvalues of H_D and by $\Pi(\lambda)$ the projector on the eigenspace of the open system relative to the energy λ , the eigenoperators of H_D can be obtained by

$$A_\alpha(\omega) = \sum_{\lambda=\lambda'} \Pi(\lambda) A \Pi(\lambda') = \sum_{k,l=1}^4 |\lambda_k\rangle \langle \lambda_l| A |\lambda_l\rangle \langle \lambda_k|. \quad (24)$$

where the sum is extended to all the couples of λ and λ' such that $\lambda - \lambda' = \omega$.

In this basis, the coherent part of the effective Hamiltonian can be expressed as $H^{(1)} = H_s + H_{Iph}$, where

$$H_s = \hbar \sum_{j=g,s,a,e} \lambda_j R_{jj} + \hbar \Omega_1 [\alpha (R_{es} + R_{ag}) + \beta (R_{sg} - R_{ea}) + H.c.]$$

$$+ \hbar \Omega_2 [\alpha (R_{ea} + R_{sg}) + \beta (R_{es} - R_{ag}) + H.c.], \quad (25)$$

and

$$H_{Iph} = \hbar \sum_{q_1} \lambda_{q_1} [R_{ee} + \beta^2 R_{ss} + \alpha^2 R_{aa} + \alpha \beta (R_{sa} + R_{as})]$$

$$\times (b_{q_1}^+ e^{i\omega_{L^1} t} + b_{q_1} e^{-i\omega_{L^1} t})$$

$$+ \hbar \sum_{q_2} \lambda_{q_2} [R_{ee} + \alpha^2 R_{ss} + \beta^2 R_{aa} - \alpha \beta (R_{sa} + R_{as})]$$

$$\times (b_{q_1}^+ e^{i\omega_{L^1} t} + b_{q_1} e^{-i\omega_{L^1} t}), \quad (26)$$

and the transformed operators are given by $R_{ij} = |i\rangle \langle j|$ ($i, j = e, a, s, g$).

We are now in a position to the derivation of the master equation for the reduced density operator of the QDs, which can be achieved by tracing the density matrix of the total system over the phonon bath operators following the standard procedure [58,60]. By assuming the Born–Markoff approximation, the density matrix of the quantum system to second order of perturbation, results in

$$\frac{\partial \rho_s}{\partial t} = -\frac{i}{\hbar} [H_s, \rho_s] - \frac{1}{\hbar^2} Tr_B \int_0^t dt' [H_{Iph}(t) H_{Iph}(t') \rho_{sB}$$

$$- H_{Iph}(t) \rho_{sB} H_{Iph}(t') + H.c.]. \quad (27)$$

Taking into account the statistical properties of the phonon baths,

$$\langle b_{q_j}^\dagger(\omega') \rangle = \langle b_{q_j}(\omega) \rangle = 0,$$

$$\langle b_{q_j}^\dagger(\omega') b_{q_j}(\omega) \rangle = n_j(\omega) \delta(\omega' - \omega),$$

$$\langle b_{q_j}(\omega') b_{q_j}^\dagger(\omega) \rangle = (n_j(\omega) + 1) \delta(\omega' - \omega), \quad (28)$$

with $n_j = 1/(\exp(\hbar\omega/K_B T) - 1)$ being the thermal average excitation numbers of the heat baths of the two QDs, a lengthy but straightforward calculation leads the reduced master equation for the atomic system (see Appendix A)

$$\frac{\partial \rho_s}{\partial t} = -\frac{i}{\hbar} [H_s, \rho_s] + L_{ph} \rho_s + L_T \rho_s, \quad (29)$$

where the Liouvillian $L_{ph} \rho_s$ is given by [32]

$$L_{ph} \rho_s = - \sum_{n=e,s,a} F_n (R_{nn} \rho_s - 2 R_{nn} \rho_s R_{nn} + \rho_s R_{nn})$$

$$- F_{sa} (R_{ss} \rho_s - 2 R_{as} \rho_s R_{sa} + \rho_s R_{ss}) - F_{as} (R_{aa} \rho_s - 2 R_{sa} \rho_s R_{as} + \rho_s R_{aa})$$

$$+ 2 C_{sa} (R_{ss} \rho_s R_{aa} + R_{aa} \rho_s R_{ss}) + 2 C_{ea} (R_{ee} \rho_s R_{aa} + R_{aa} \rho_s R_{ee})$$

$$+ 2 C_{es} (R_{ee} \rho_s R_{ss} + R_{ss} \rho_s R_{ee}). \quad (30)$$

The coefficients F_{ij} ($j = a, s, e, g$) in Eq. (30) represent different decay rates of the states $|\lambda_e\rangle$, $|\lambda_s\rangle$ and $|\lambda_a\rangle$ and the coefficients C_{ij} are cross

decay terms involving diagonal matrix density terms. The most relevant terms for the current work are the decay rates F_{sa} and F_{as} which describe the bath-induced transition rate from $|\lambda_s\rangle$ to $|\lambda_a\rangle$, and from $|\lambda_a\rangle$ to $|\lambda_s\rangle$, respectively. We will see later on that the imbalance between this decay rates gives rise to the enhancement of entanglement between the QDs. The different coefficients in Eq. (30) are given by

$$F_e = [n_1(\omega_{q_1}) + n_2(\omega_{q_1}) + 2] \Gamma_{pn},$$

$$F_s = \beta^4 [n_1(\omega_{q_1}) + 1] \Gamma_{pn} + \alpha^4 [n_2(\omega_{q_2}) + 1] \Gamma_{pn},$$

$$F_a = \alpha^4 [n_1(\omega_{q_1}) + 1] \Gamma_{pn} + \beta^4 [n_2(\omega_{q_2}) + 1] \Gamma_{pn},$$

$$C_{es} = \beta^2 [n_1(\omega_{q_1}) + 1] \Gamma_{pn} + \alpha^4 [n_2(\omega_{q_2}) + 1] \Gamma_{pn},$$

$$C_{ea} = \alpha^2 [n_1(\omega_{q_1}) + 1] \Gamma_{pn} + \beta^4 [n_2(\omega_{q_2}) + 1] \Gamma_{pn},$$

$$C_{as} = \alpha^2 \beta^2 [n_1(\omega_{q_1}) + n_2(\omega_{q_2}) + 2] \Gamma_{pn},$$

$$F_{sa} = \alpha^2 \beta^2 [n_1(2J_{eff}) + n_2(2J_{eff}) + 2] \Gamma_{pn},$$

$$F_{as} = \alpha^2 \beta^2 [n_1(2J_{eff}) + n_2(2J_{eff})] \Gamma_{pn}. \quad (31)$$

Here, $\Gamma_{pn} = \sum_{j=1,2} \sum_{qj} \left(\frac{\lambda_{qj}}{\hbar}\right)^2 \delta(\omega_{qj} - 2J_{eff})$ is the dissipation rate induced by the electron–phonon coupling [61] and thus may reveal the influence of the phonon participation processes on the entanglement between the two QDs.

On the other hand, the Liouvillian due to the interaction with the vacuum and cavity modes L_T is [62]

$$L_T \rho_s = -\Gamma_s [(R_{ee} + R_{ss}) \rho_s + \rho_s (R_{ee} + R_{ss}) - 2 R_{se} \rho_s R_{es} - 2 R_{gs} \rho_s R_{sg}]$$

$$+ 2 (\alpha \beta \gamma + \Gamma_{12}) (R_{es} \rho_s R_{sg} + R_{gs} \rho_s R_{es})$$

$$- \Gamma_a [(R_{ee} + R_{aa}) \rho_s + \rho_s (R_{ee} + R_{aa}) - 2 R_{ae} \rho_s R_{ea} - 2 R_{ga} \rho_s R_{ag}]$$

$$- 2 (\alpha \beta \gamma - \Gamma_{12}) (R_{ae} \rho_s R_{ag} + R_{ga} \rho_s R_{ea})$$

$$- 2 \Gamma_{as} [(R_{as} + R_{sa}) \rho_s + (R_{ga} \rho_s R_{sg} + R_{gs} \rho_s R_{sg} + R_{se} \rho_s R_{ea} + R_{ae} \rho_s R_{es})]$$

$$- (\alpha^2 - \beta^2) \gamma (R_{ae} \rho_s R_{sg} + R_{gs} \rho_s R_{ea} + R_{se} \rho_s R_{ag} + R_{se} \rho_s R_{ag} + R_{ga} \rho_s R_{es}), \quad (32)$$

with

$$\Gamma_a = \frac{1}{2} (\Gamma_1^M + \gamma - 2\alpha\beta\Gamma_{12}),$$

$$\Gamma_s = \frac{1}{2} (\Gamma_1^M + \gamma + 2\alpha\beta\Gamma_{12}),$$

$$\Gamma_{as} = \frac{1}{2} (\alpha^2 - \beta^2) \Gamma_{12}. \quad (33)$$

The coefficients Γ_a , and Γ_s are the spontaneous emission rates of the transitions. The interference term proportional to Γ_{as} results from spontaneously induced coherences between the symmetric and anti-symmetric transitions [62]. This term appears only in systems of atoms with different transition frequencies, i.e. $\Delta_0 \neq 0$. It is worth noting that if we take $\Omega_1 = \Omega_2 = 0$, and $\kappa = 0$, and the atoms have the same transition frequency ($\Delta_0 = 0$), Eq. (29) reduces to the results presented in [47]. Here we incorporate the effects of the plasmonic cavity, the phonon baths and the presence of an external driving field. In the following we shall analyze the influence of the phonon environment on entangled creation between the two QDs in presence of the MNP and the external coherent field, for identical ($\Delta_0 = 0$) and nonidentical ($\Delta_0 \neq 0$) atoms.

3. Numerical results

For illustration of the numerical results, we choose a realistic hybrid system consisting of two quantum dots near the MNP. We consider a spherical gold MNP with radius $a = 6$ nm, plasma frequency $\omega_p = 8.54$ eV, damping constant $\gamma_p = 0.054$ eV, and high-frequency limit $\epsilon_\infty = 9.45$ [55]. With these parameters, the Drude model assumed in Eq. (2) provides a reasonably good fit to tabulated experimental data for photon energies smaller than 3 eV. The dielectric constant of the host material is taken as $\epsilon_B = 2.25$. The dipole moment and decay rate of the QD in vacuum are set to $\mu_{eg} = 0.7e$ nm and $\gamma_{11} = \gamma_{22} \equiv \gamma = 60$ μ eV. The distances $R_1 = R_2$ are set to 14 nm, unless otherwise stated. Using these experimental data we obtain from Eq. (8), $g_1 = g_2 = 3.32$ meV,

and $\kappa = 54.96$ meV. [63]. In addition the dipole–dipole interaction J_D takes the form $J_D = S_\alpha \frac{\mu_{eg}^{(1)} \mu_{eg}^{(2)}}{4\pi\epsilon_0 \hbar (R_1 + R_2)^3}$. Substituting the different parameters we obtain $J_D = 0.06$ eV.

The interaction with the phonon reservoir can be characterized by the dissipation rate induced by the electron–phonon coupling, $\Gamma_{pn} = \sum_{j=1,2} \sum_{qj} \left(\frac{\lambda_{qj}}{\hbar} \right)^2 \delta(\omega_{qj} - 2J_{eff})$ given in Eq. (31). Here we adopt the established phonon spectral function, $\Gamma_{pn} \simeq \frac{\hbar A}{\pi k_B} \omega^3 \exp(-\frac{\omega^2}{2\omega_{cut}^2})|_{\omega=2J_{eff}}$, which describes the electron–acoustic-phonon interaction via a deformation potential, the dominant source of phonon scattering for InAs and GasAs QDs [64,65]. Here ω_{cut} is a cutoff frequency, A is a parameter that reflects the dissipation strength [66–68], and for the current system, $\omega \simeq 2J_{eff}$. We take typical values for $A \simeq 11$ fs/K, and $\hbar\omega_{cut} \simeq 1.44$ meV, which have been extracted experimentally for a GaAs/InGaAs quantum dot [67]. On the other hand $J_{eff} = S_\alpha \frac{\mu_{eg}^{(1)} \mu_{eg}^{(2)}}{4\pi\epsilon_0 \hbar R^3} + \frac{g_1 g_2 \delta_e}{\kappa^2/4 + \delta_e^2}$. By assuming $R \simeq \lambda$, we obtain $J_{eff} \simeq 1.3 \times 10^{12}$ Hz. Substituting this value in the expression for the damping parameter Γ_{ph} , we obtain values of the order of $\Gamma_{ph} = 2.5\gamma$.

We are interested in how the amount of entanglement varies when the phonon reservoirs with temperature T are introduced. We begin by exploring a situation in which the temperature of the baths is the same ($T_1 = T_2$) and is set near to zero, so the occupation numbers $n_j(\omega_{qj}) \simeq 0$ in Eq. (31). Later we shall release this restriction. To quantify the grade of entanglement of a two-qubit system we use the concurrence C defined as [69]

$$C = \max\{0, \sqrt{\lambda_1} - \sqrt{\lambda_2} - \sqrt{\lambda_3} - \sqrt{\lambda_4}\}, \quad (34)$$

λ 's being the eigenvalues, in a decreasing order, of the matrix $\tilde{\rho} = \rho_{\sigma_y} \otimes \sigma_y \rho^* \otimes \sigma_y$, where ρ^* denotes the complex conjugation of ρ , and σ_y is the y -component of the Pauli matrix. The case of $C = 1$ corresponds to the existence of the maximum entanglement between the two qubits, and $C = 0$ means no entanglement between the qubits.

To see the dynamical phenomena of entanglement, in Fig. 2, the dynamical evolution of the concurrence as a function of γt is displayed with and without the presence of the phonon baths for different non-entangled initial states, namely $\psi_1(0) = |gg\rangle$, $\psi_2(0) = |ee\rangle$, $\psi_3(0) = |eg\rangle$ and finally we will consider a Bell state which is a maximally entangled state $|\Psi_4(0)\rangle = \frac{1}{\sqrt{2}}[|eg\rangle + |eg\rangle]$.

For the case of $\Psi_1(0) = |gg\rangle$ we can see in Fig. 2a that in absence of phonon interaction ($\Gamma_{pn} = 0$), the concurrence rise to a maximum and then reaches a non-null steady-state ($C \simeq 0.2$) (solid curve). The result is very different if the phonon bath is accounted for. For example, for $\Gamma_{pn} = 2.5\gamma$, after a sudden death period, the concurrence duplicates the steady value (dashed curve).

Now, we turn our attention to the case where $\Psi_2(0) = |ee\rangle$, i.e., the two quantum dots are in their excited state. In both cases without and with phonons (Fig. 2b), sudden birth of entanglement takes place because in order to become entangled, one or both atoms have to decay to the ground state. We observe the so-called sudden birth of entanglement starting at different times. These processes depend on both the individual QD decay rate and the collective decay rate Γ_{12}^M , which are modified by the presence of phonons.

Fig. 2c displays the concurrence for the case of $\Psi_3(0) = |eg\rangle$, i.e. one QD is in the excited state and the other one is on the ground state. We can see again that in absence of phonon interaction ($\Gamma_{pn} = 0$), the concurrence rise to a maximum and then becomes zero, and experience a sudden death for a time range before reviving shortly after, reaching a low steady-state value (solid curve). The result is very different if the phonon bath is accounted for. For example, for $\Gamma_{pn} = 2.5\gamma$, entanglement persists along the time and the concurrence is clearly enhanced (dashed curve).

Finally, we consider now how the presence of phononic baths affects the loss of entanglement in the case of starting from a maximally entangled state, $|\Psi_4(0)\rangle = \frac{1}{\sqrt{2}}[|eg\rangle + |eg\rangle]$. Realization of Bell states in QDs has been proposed via excitons in a single dot [70] or in coupled

QDs [71]. It is worth noting that different methods for creating entangled states have been proposed recently. In particular STIRAP methods for generating a specific type of two-qubit where the interqubit coupling there was taken of a separable entangled state, has been described in Refs. [72,73]. In addition, concerning to the system considered in this work, where the mutual interqubit interaction is chosen to be of a Heisenberg-type exchange character, it has been shown that a system of two identical two-level atoms may be prepared in the symmetric state by a short laser pulse [74], and by rapid adiabatic passage (RAP) with chirped Gaussian pulses [75,76].

In order to show how an initially maximal entangled state $|\Psi_4(0)\rangle = \frac{1}{\sqrt{2}}[|eg\rangle + |eg\rangle]$ can be prepared, we consider the Hamiltonian given in Eq. (18) where the atoms are driven by a chirped Gaussian pulse given by $\Omega(t) = \Omega_0 e^{-t^2/(2\tau^2)} e^{i(\omega_L t + b/2t^2)}$, where b is the chirp parameter, Ω_0 defines the pulse amplitude, τ its duration, and ω_L its central frequency. We take a pulse of $\tau = 4$ ps, so that we can ignore in a first approximation the QDs decay processes, which are of the order of several hundred picoseconds. To analyze the dynamics of the system we normalize the different parameters to the pulse duration, i.e. we define the dimensionless parameters $b\tau^2$, $\Omega_0\tau$, and $J_{eff}\tau$, and we consider identical QDs, i.e. $\Delta_0 = 0$.

Fig. 3a shows the population dynamics during the excitation with $\Omega_0 = 5\tau$, $b = -2\tau^2$ and $\Delta_L = -J\tau$. Before the laser pulse, the system is in the ground state $|gg\rangle$. During the pulse ρ_{gg} drops down (dashed line), while a transient occupation of the collective state ρ_{ss} occurs. Around $t = 0$ a population transfer to the collective excited state $|e\rangle = |ee\rangle$ takes place. Finally, the $|s\rangle$ state is almost completely occupied. Fig. 3b shows the concurrence C as a function of the dimensionless parameters $b\tau^2$, and $J\tau$ in the resonant case $\Delta_0 = 0$. It can be seen that maximum value of concurrence can be obtained over a wide range of values of chirp and coupling. From Fig. 3b we can maximum entangled state can be obtained for a value of $J_{eff}\tau$ in the range $1 < J_{eff}\tau < 4$, i.e. $J_{eff} \simeq 4/4ps \simeq 10^{12}$ Hz, which is compatible with the J_{eff} values reached in our system, in the order of 1.2×10^{12} Hz.

Once the initial state is prepared, we apply a constant amplitude field over time to see the time evolution of the concurrence when the system is initially in a maximally entangled state in absence and in presence of phononic baths. Fig. 3c shows that unlike the other cases, both curves for $t = 0$ have unity C since our initial state is maximally entangled state. At early times, in both cases the concurrence decreases which means a considerable loss of entanglement and for the case of $\Gamma_{PH} = 2.5$, we observe the so-called sudden death of entanglement followed by a revival (dashed line). However, at long times reaches a steady-state value greater than the value obtained in the case of $\Gamma_{PH} = 0$. We can conclude that in this regime of temperatures, the entanglement loss is lower than in the case without phonons.

In summary, an overall comparison of all considered initial states in Figs. 2 and 3 reveals that the quantum correlations between the QDs, expressed with the concurrence C are enhanced when the phononic baths are taking into account. Of course the reached steady-state concurrence is the same value, independently of the initial state.

In order to explain the numerical results displayed in Fig. 2, it is useful to analyze the evolution of populations of the symmetric and antisymmetric states, since a direct expression for concurrence can be obtained in the case of weak driving field [77]. We focus in the case in which the initial state is $\Psi(0) = |eg\rangle$, since a direct expression for concurrence can be obtained for a weak driving field [77]:

$$C \simeq \sqrt{(\rho_{ss} - \rho_{aa})^2 + 4Im(\rho_{as})} - 2\sqrt{(\rho_{gg} - \rho_{ee})}. \quad (35)$$

This equation tell us that the greater the difference in populations $\rho_{ss} - \rho_{aa}$, the greater the concurrence, so we will have to try to populate the symmetric or antisymmetric state with a high probability.

In Fig. 2c we have considered the case $\Delta_L = \Delta_0 = 0$, i.e., the QDs have the same transition frequency. Therefore, from Eq. (22) we obtain $\alpha = \beta = 1/\sqrt{2}$ and the decay rates take the values $\Gamma_{as} = 0$,

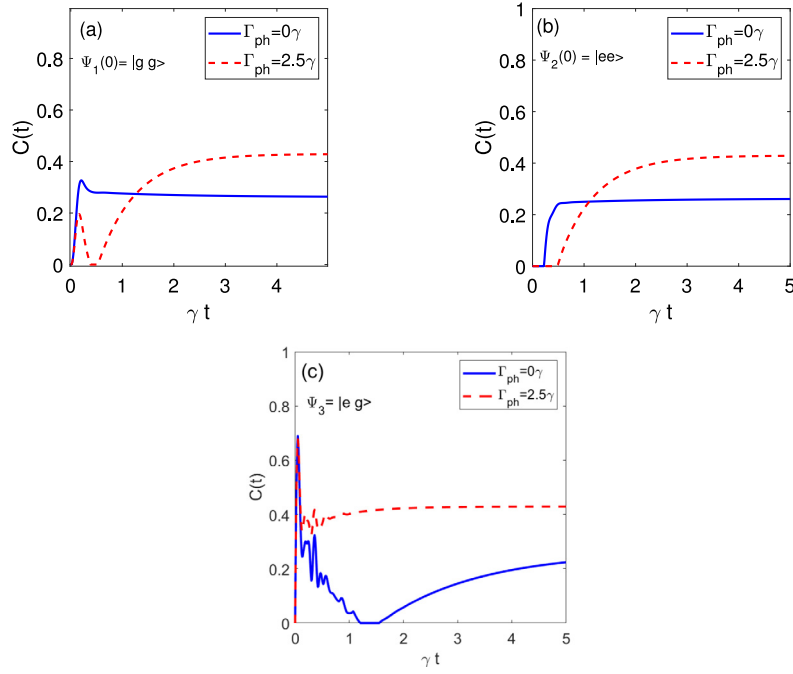


Fig. 2. Time evolution of the concurrence of the two qubits for different phonon strengths $\Gamma_{ph} = 0$ (solid curve), $\Gamma_{ph} = 2.5\gamma$ (dashed curve), and different initial states: (a) $|\Psi(0) = |gg\rangle$, (b) $|\Psi(0) = |ee\rangle$, and (c) $|\Psi(0) = |eg\rangle$.

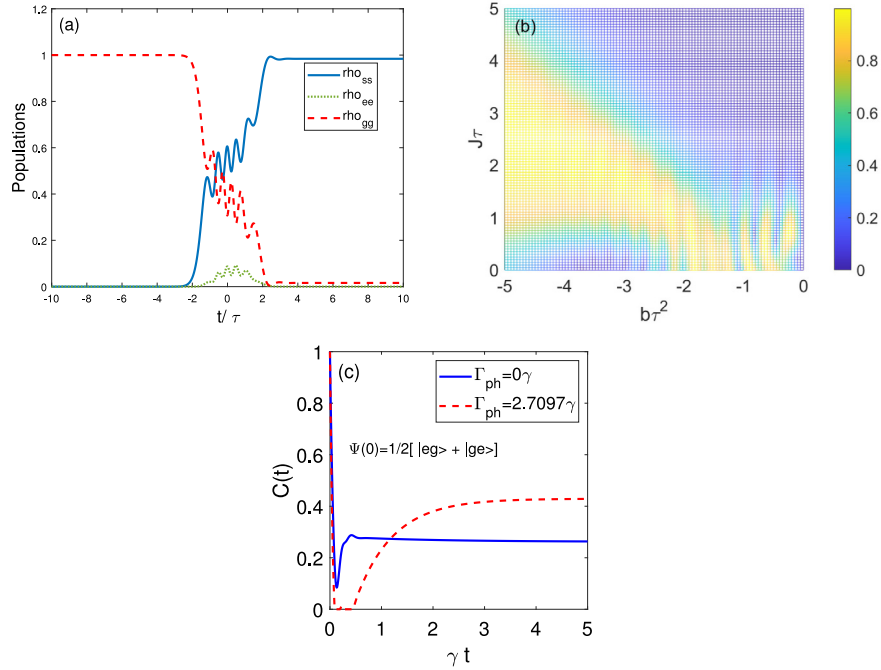


Fig. 3. (a) Final occupation of the states $|g\rangle$ (dashed line), $|s\rangle$ (solid line), and $|e\rangle$ (dotted line), after excitation with a laser pulse with pulse amplitude $\Omega_0 = 5\tau$ and chirp coefficient $b = -2\tau^2$. (b) Concurrence as a function of the dimensionless linear chirp, $b\tau^2$, and coupling $J\tau$ in the case $A_0 = 0$ and $\Omega_0 = 5\tau$. (c) Time evolution of the concurrence of the two qubits for different phonon strengths $\Gamma_{ph} = 0$ (solid curve), $\Gamma_{ph} = 2.5\gamma$ (dashed curve) after excitation with a constant field and initial state $|\Psi(0) = \frac{1}{2} [|eg\rangle + |ge\rangle]$.

$\Gamma_1^M = \Gamma_2^M = \Gamma^M$, and $\Gamma_{12}^M = \Gamma_{21}^M$. In addition we have assumed that $\Omega_1 = \Omega_2$. Thus, from the derived Hamiltonian in the Dicke basis (Eq. (25)), we can obtain the time evolution of the symmetrical and antisymmetrical populations given by (see Appendix B)

$$\begin{aligned}\dot{\rho}_{ee}(t) &= -2(\Gamma_s + \Gamma_a)\rho_{ee}, \\ \dot{\rho}_{ss}(t) &= -2(\Gamma^M + \Gamma_{12}^M + \gamma + F_{sa})\rho_{ss} + 2\Gamma_s\rho_{ee}\end{aligned}$$

$$\begin{aligned}&+ i\frac{2}{\sqrt{2}}\Omega_1(\rho_{se} - \rho_{es}) + i\frac{2}{\sqrt{2}}\Omega_1(\rho_{sg} - \rho_{gs}), \\ \dot{\rho}_{aa}(t) &= -2(\Gamma^M - \Gamma_{12}^M + \gamma + F_{as})\rho_{aa} + 2F_{sa}\rho_{ss} + 2\Gamma_a\rho_{ee}.\end{aligned}\quad (36)$$

The decay processes in Eqs. (36) can be represented for collective levels as in Fig. 4d. It is clear that two cascade channels $|e\rangle \rightarrow |s\rangle \rightarrow |g\rangle$ and $|e\rangle \rightarrow |a\rangle \rightarrow |g\rangle$, which are shown in Fig. 4(d), have different decay

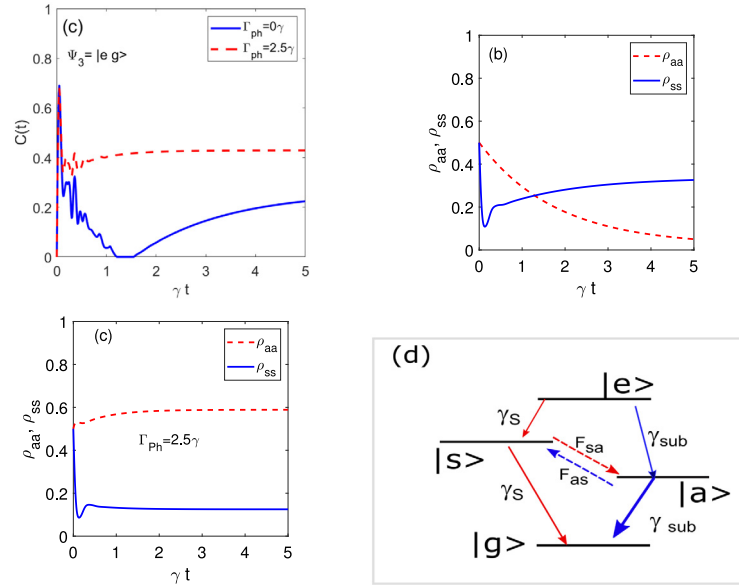


Fig. 4. (a) Time evolution of the concurrence of the two qubits for different phonon strengths $\Gamma_{ph} = 0$ (solid curve), $\Gamma_{ph} = 2.5\gamma$ (dashed curve) for the initial state $|\Psi_3(0) = |eg\rangle$. (b) Time evolution of the symmetric (solid) and antisymmetric state population (dashed) for $\Gamma_{ph} = 0$. (c) Time evolution of the symmetric (solid) and antisymmetric state population (dashed) for $\Gamma_{ph} = 2.5\gamma$. Other parameters are: $\gamma = 60\mu$, $\delta_c = 2 \times 10^2\gamma$, $\Delta_L = 0$, and $\Delta_0 = 0$ eV $\kappa = 54.96$ meV, and $g_1 = g_2 = 3.32$ meV. (d) Decay processes in the Dicke basis. The two-qubit cooperative states are $|\Phi_i\rangle$ where $(i = e, s, a, g)$, stand for excited, symmetrical, antisymmetrical and ground Dicke states, respectively. The superradiant and subradiant decay rates are: $\gamma_s = \Gamma^M + \gamma + 2\alpha\beta\Gamma_{12}^M$ and $\gamma_{sub} = \Gamma^M + \gamma - 2\alpha\beta\Gamma_{12}^M$.

rates: the symmetric transitions decay with an enhanced (superradiant) rate $\gamma_s = \Gamma^M + \gamma + 2\alpha\beta\Gamma_{12}^M$, whereas the antisymmetric transitions decay with a reduced (subradiant) rate $\gamma_{sub} = \Gamma^M + \gamma - 2\alpha\beta\Gamma_{12}^M$. More interestingly, the interaction with the phonon subsystem opens two additional decay channels, one is channel $|s\rangle \rightarrow |a\rangle$ with a decay rate F_{sa} , and the other is $|a\rangle \rightarrow |g\rangle$ with a decay rate F_{as} . Fig. 4(b) displays the dynamical evolution of populations ρ_{ss} and ρ_{aa} in absence of phonon bath, i.e. $\Gamma_{ph} = 0$. It can be seen that at early times, the populations are very different, which leads to a high value of the concurrence (see Eq. (35)). Then, at certain time both populations become equal, which is related to the appearance of the sudden death. For long times the symmetrical and antisymmetrical states tend to populate almost equal, keeping their difference to a low value. This can be qualitatively explained as follows: since $F_{sa} = \alpha^2\beta^2 [n_1(2J_{eff}) + n_2(2J_{eff}) + 2] \Gamma_{ph}$ and $F_{as} = \alpha^2\beta^2 [n_1(2J_{eff}) + n_2(2J_{eff})] \Gamma_{ph}$, for the case $\Gamma_{ph} = 0$, we have $F_{as} = F_{sa} = 0$, and the decay channels $|s\rangle \rightarrow |a\rangle$ and $|s\rangle \rightarrow |g\rangle$ disappear. In addition, the term proportional to $2F_{sa}\rho_{ss}$ in Eq. (36) for $\dot{\rho}_{aa}$, which represents a pumping term, also disappears. Thus the difference $|\rho_{aa} - \rho_{ss}|$ is near to zero. However when the phonon coupling is accounted for ($\Gamma_{ph} = 2.5\gamma$), Fig. 4(c) clearly shows that population tends to accumulate in the antisymmetric state ρ_{aa} , and more importantly, the difference $|\rho_{aa} - \rho_{ss}|$ is always greater than the case with $\Gamma_{ph} = 0$. This fact is responsible for the enhancement of the concurrence appearing in Fig. 2. Therefore, the enhancement of the concurrence can be explained by the fact that phonons change the effective decay rates of the transitions between the collective states: for the case $\Gamma_{ph} = 2.5\gamma$, $F_{sa} \gg F_{as}$, the decay channel $|e\rangle \rightarrow |a\rangle$ is activated and the antisymmetrical state gets more populated than the symmetrical one. In general, any difference between the decay processes between the transitions $|e\rangle \rightarrow |s\rangle \rightarrow |g\rangle$ and $|e\rangle \rightarrow |a\rangle \rightarrow |g\rangle$ will affect the concurrence. Note that F_{sa} and F_{as} depend on external parameters such as Δ_0 , Δ_L and Ω_j , among others, so concurrence can be controlled by changing them. This will be accomplished in the following.

A more general behavior of the temporal evolution of the concurrence for different values of the Rabi frequency of the driving field is displayed in Fig. 5. In absence of coupling to the phonons (Fig. 5(a)), concurrence values rise to a maximum for early time and then go

to zero for low values of the Rabi frequency. When Rabi frequency increases, a low steady-state value is reached after sudden death entanglement. For high Rabi frequency values, concurrence is near zero. The entanglement is substantially enhanced when the coupling with phonons is accounted for. If we compare with the results displayed in Fig. 5(b), we can see that entanglement appears for all time instants and concurrence values of the order of 0.5 are achieved for a large set of Rabi frequency. In sort, the presence of phonons, at this level, improves the concurrence and therefore the entanglement at steady-state.

Now we analyze the influence of external parameters such as the detuning of the driving field and the transition frequency of the QDs. In Fig. 6(a) the concurrence versus γt , for different detunings Δ_L is displayed. We can see that the steady-state concurrence reach a maximum value for $\Delta_L = -13\gamma$, i.e. when $\Delta_L = -J_{eff}$.

Until now we have assumed that the QDs have the same transition frequency ($\Delta_0 = 0$). However it is technically challenging to have two separate QDs with the same resonance frequency due to their wide spectral variations, making it extremely unlikely that two QDs will be resonant with the external field simultaneously [78]. In Fig. 6(b) we analyze this nonsymmetric situation in which the two QDs have different transition frequencies, i.e. $\Delta_0 \neq 0$. In this case, it is evident from Eq. (22) that different values of Δ_0 change the values of the parameters α and β , which determine the final values of the decay rates given in Eqs. (31). Here we observe that maximum concurrence occurs for the case of identical atoms ($\Delta_0 = 0$), decreasing to zero as the difference between its frequencies increases. The reason is again due to the difference between the decay processes between the transitions $|e\rangle \rightarrow |s\rangle \rightarrow |g\rangle$ and $|e\rangle \rightarrow |a\rangle \rightarrow |g\rangle$, as shown in Fig. 6c, where F_{sa} and F_{as} are displayed versus Δ_0 . The difference between both decays reaches a maximum value at $\Delta_0 = 0$ and then decreases to zero for high values of Δ_0 . This explains the fact that concurrence decreases for nonidentical atoms.

In order to check the robustness of the entanglement against variations of plasmonic cavity parameters κ and δ_c , the temporal evolution of the concurrence is shown in Fig. 7. It can be seen that the steady-state concurrence remains relatively high even if the values of κ change for an order of magnitude (Fig. 7a). Similar results occur for changes

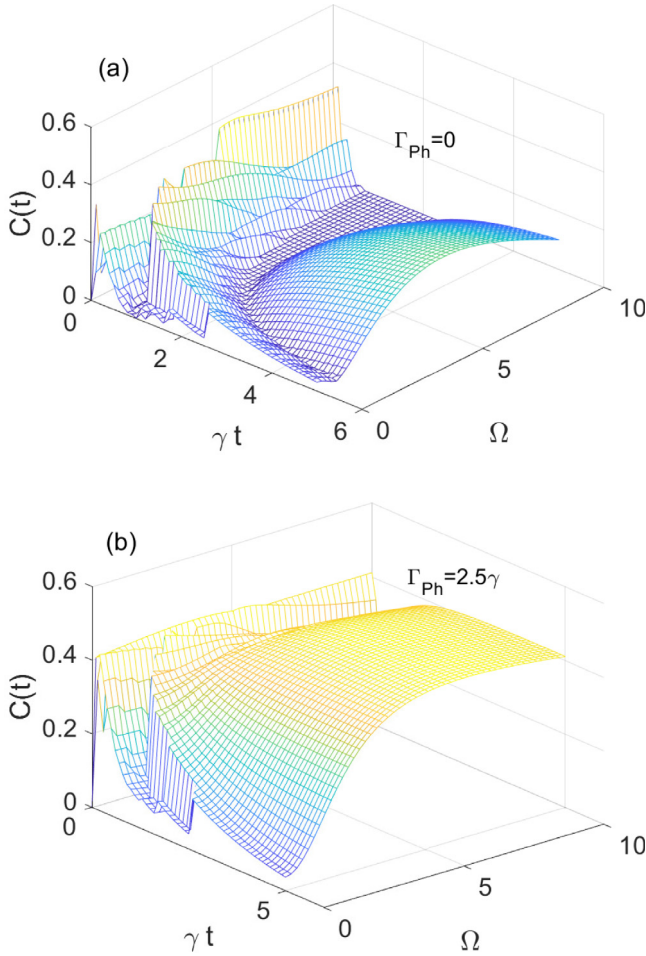


Fig. 5. (a) Concurrence versus time and Rabi frequency of the driving field without phonons ($\Gamma_{ph} = 0$). (b) Concurrence versus time and Rabi frequency of the driving field in presence of phonons ($\Gamma_{ph} = 2.5\gamma$). The initial state is $|\Psi_3(0) = |eg\rangle$. Other parameters are: $\delta_c = 2 \times 10^2 \gamma$, $\kappa = 9 \times 10^2 \gamma$, and $g_1 = g_2 = 50\gamma$, $\Delta_L = 0$, and $\Delta_0 = 0$.

in the detuning δ_c (Fig. 7(b)). However when the cavity detuning δ_c is large (dashed curve), the plasmonic cavity is far of resonance with the driving field, and concurrence decreases significantly.

The above results have been obtained considering a phonon baths temperatures near to zero. In order to analyze the dependence with the temperature Fig. 8(a) displays temporal evolution of the concurrence for different temperatures of the phononic bath. In this case, all decay terms in Eq. (31) all terms grow because of their dependency on the thermal average excitation numbers $n_j = 1/(\exp(\hbar\omega/K_B T) - 1)$ of the heat baths. As might be expected, we observe that when the temperature T_B of the bath increases, the concurrence decreases at all times. For $T_B > 10K$, concurrence is lower than the one obtained without phonons (green curve). Fig. 8(b) also shows that the steady-state concurrence decreases from a maximum value of 0.4 to 0 as the temperature T_B increases above $T_B > 30K$. This occurs because the mean number of phonons of both reservoirs for $T_B > 30K$ reaches high values, i.e. $n_1 = n_2 \gg 1$. Moreover this implies that the decay rates F_{sa} and F_{as} between the subradiant and superradiant states reach the same value, i.e., $F_{sa} \simeq F_{as}$. In this situation, populations ρ_{aa} and ρ_{ss} reach the same values, and concurrence tends to zero. The dashed line indicates the maximum value of the concurrence in absence of phonons. Therefore, the enhancement induced by the phonon environment is only effective at low temperatures. For higher temperatures, the phonon bath destroys the entanglement.

4. Discussion and summary

In summary, we have analyzed the entanglement between two qubits near a MNP driven by a coherent field taking into account the coupling with a phonon environment. An effective Hamiltonian for the atomic subsystem is derived by adiabatically eliminating the plasmonic cavity modes, which allows us to solve the master equation for the qubits. We have shown that steady-state entanglement can be enhanced by the coupling with a phonon bath for some range of temperatures. We have explained the underlying physical mechanisms based in terms of the induced transitions among the symmetrical and antisymmetrical two-qubit collective states. We have analyzed the effects on entanglement for different parameters, which can be experimentally controlled. In particular, it is found that concurrence can be modified by appropriately tuning qubit detunings and the driving Rabi frequency. Further, the entanglement is found to be robust against small perturbations in the transition frequencies of the QDs and the frequency of the driving field. We have verified that the concurrence is not destroyed through the interaction with the environment and that it remains stable for proper range of temperatures. As a consequence, it is possible to control the dynamic evolution of two qubits and the entanglement generation and preservation, which may have important applications in controllable quantum devices.

Declaration of competing interest

The authors declare that they have no known competing financial interests or personal relationships that could have appeared to influence the work reported in this paper.

Acknowledgments

I acknowledge T. Lorca and I. Gonzalo for fruitful discussion. This work is supported by project FIS2017-87360-P (MICINN), Spain.

Appendix A. Derivation of the liouvillian $L_{ph}\rho$

From Eq. (27), the Liouvillian due to the interaction with the phonon environments is given by

$$L_{ph}\rho_s \equiv -\frac{1}{\hbar^2} Tr_B \int_0^t dt' [H_{Iph}(t)H_{Iph}(t')\rho_{s_B} - H_{Iph}(t)\rho_{s_B}H_{Iph}(t') + H.c.] \quad (A.1)$$

where ρ_{s_B} is the matrix density of the complete system and H_{Iph} given by

$$\begin{aligned} H_{Iph}(t) &= \hbar \sum_{q_1} \lambda_{q_1} [R_{ee} + \beta^2 R_{ss} + \alpha^2 R_{aa} + \alpha\beta(R_{sa} + R_{as})] \\ &\times (b_{q_1}^+ e^{i\omega_L t} + b_{q_1} e^{-i\omega_L t}) \\ &+ \hbar \sum_{q_2} \lambda_{q_2} [R_{ee} + \alpha^2 R_{ss} + \beta^2 R_{aa} - \alpha\beta(R_{sa} + R_{as})] \\ &\times (b_{q_1}^+ e^{i\omega_L t} + b_{q_1} e^{-i\omega_L t}), \end{aligned} \quad (A.2)$$

We introduce the notations

$$A_j(t) = \hbar \sum_{q_j} \lambda_{q_j} (b_{q_j}^+ e^{i\omega_L t} + b_{q_j} e^{-i\omega_L t}) \quad (j = 1, 2), \quad (A.3)$$

so the Eq. (A.2) can be cast as

$$\begin{aligned} H_{Iph}(t) &= R_{ee} [A_1(t) + A_2(t)] + R_{ss} [\beta^2 A_1(t) + \alpha^2 A_2(t)] \\ &+ R_{aa} [\alpha^2 A_1(t) + \beta^2 A_2(t)] \\ &+ \alpha\beta [A_1(t) - A_2(t)] [R_{sa} + R_{as}], \end{aligned} \quad (A.4)$$

Inserting Eq. (A.4) in Eq. (A.1) we obtain

$$L_{ph}\rho_s = Tr_B \int_0^t dt' [R_{ee}(t)\rho_{s_B}(t)B_{ee}(t')B_{ee}(t') + R_{ss}(t)\rho_{s_B}(t)B_{ss}(t')B_{ss}(t')]$$

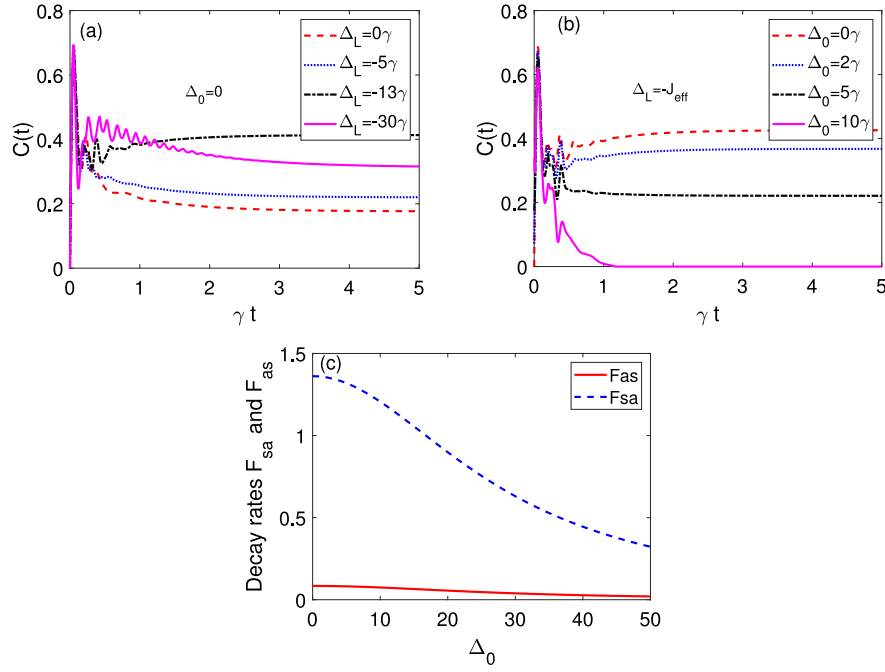


Fig. 6. (a) Time dependence of the concurrence between the two qubits for different detuning Δ_L between the driving field and the QD transition: $\Delta_L = 0$ (dashed curve), $\Delta_L = -5\gamma$ (dotted curve), $\Delta_L = -13\gamma$ (dashed-dotted curve), and $\Delta_L = -30\gamma$ (solid curve) and identical atoms ($\Delta_0 = 0$). (b) Time dependence of the concurrence between the two qubits for $\Delta_L = -J_{eff}$ and different detunings Δ_0 (nonidentical atoms): $\Delta_0 = 0$ (solid curve), $\Delta_0 = 2\gamma$ (dashed curve), $\Delta_0 = 5\gamma$ (dotted curve), and $\Delta_0 = 10\gamma$ (dashed-dotted). (c) The decay emission damping rates F_{sa} and F_{as} a function of Δ_0 . Phonon strength $\Gamma_{ph} = 2.5\gamma$ and $\Delta_L = -J_{eff} = -13\gamma$. The initial state is $|\Psi_3(0)\rangle = |eg\rangle$. Other parameters as in Fig. 2.

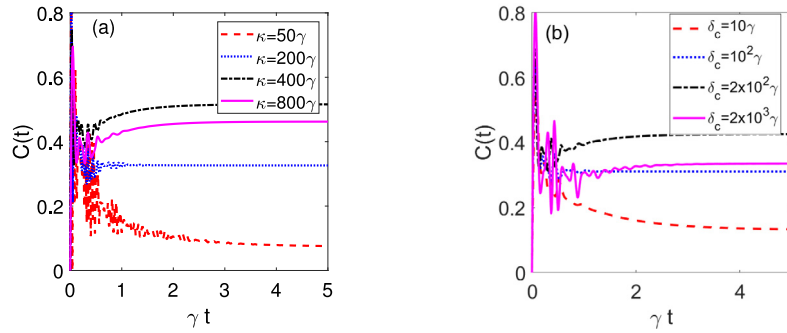


Fig. 7. Time dependence of the concurrence C in presence of phonons ($\Gamma_{ph} = 2.5\gamma$) between the two qubits for different plasmonic cavity decay parameter: (a) $\kappa = 50\gamma$ (dashed line), $\kappa = 200\gamma$ (dotted), $\kappa = 400\gamma$ (dashed-dotted) and $\kappa = 800\gamma$ (solid). (b) Dependence of the concurrence C on the plasmonic cavity detuning: $\delta_c = 10\gamma$ (dashed line), $\delta_c = 100\gamma$ (dotted), $\delta_c = 200\gamma$ (dashed-dotted), and $\delta_c = 2000\gamma$ (solid). The initial state is $|\Psi_3(0)\rangle = |eg\rangle$.

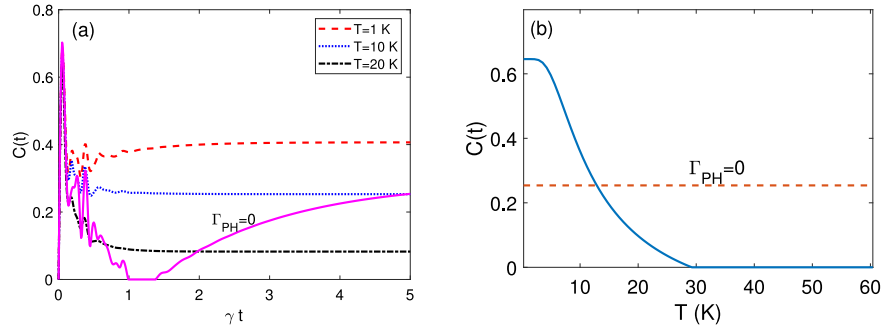


Fig. 8. (a) Time dependence of the concurrence C between the two qubits for different bath temperatures and an initial state $|\Psi_3(0)\rangle = |eg\rangle$: $T = 1\text{ K}$ (dashed line), $T = 10\text{ K}$ (dotted), $T = 20\text{ K}$ (dashed-dotted). For comparison purposes, the solid line represents the case in absence of phonon bath. (b) Steady-state concurrence versus bath temperature for $\Omega_1 = \Omega_2 = 5\gamma$, $\Delta_0 = 0$, $\Delta_L = -J_{eff}$, $\Gamma_{ph} = 2.5\gamma$ and the rest of parameters as in Fig. 2. The dashed line indicates the maximum value of the concurrence in absence of phonons ($\Gamma_{PH} = 0$).

$$\begin{aligned}
& R_{aa}(t)\rho_{s_B}(t)B_{aa}(t') - R_{ee}(t)\rho_{s_B}(t)R_{ee}(t')B_{ee}(t') \\
& - R_{ss}(t)\rho_{s_B}(t)R_{ss}(t')B_{ee}(t') + R_{aa}(t)\rho_{s_B}(t)R_{aa}(t')B_{aa}(t') \\
& - Tr_B \int_0^t dt' [R_{ee}(t)B_{ee}(t')\rho_{s_B}(t)R_{ss}(t')B_{ss}(t') \\
& + R_{ee}(t)B_{ee}(t')\rho_{s_B}(t)R_{aa}(t')B_{aa}(t') \\
& + R_{ss}(t)B_{ss}(t')\rho_{s_B}(t)R_{ee}(t')B_{ee}(t') + R_{ss}(t)B_{ss}(t')\rho_{s_B}(t)R_{aa}(t')B_{aa}(t') \\
& + R_{aa}(t)B_{aa}(t')\rho_{s_B}(t)R_{ee}(t')B_{ee}(t') + R_{aa}(t)B_{aa}(t')\rho_{s_B}(t)R_{ss}(t')B_{ss}(t') \\
& + Tr_B \int_0^t dt' [R_{sa}(t)R_{as}(t')\rho_{s_B}(t)B_{sa}(t)B_{as}(t') \\
& + R_{as}(t)B_{as}(t')\rho_{s_B}(t)R_{sa}(t')B_{sa}(t')] \\
& - Tr_B \int_0^t dt' [R_{sa}(t)B_{sa}(t')\rho_{s_B}(t)R_{as}(t')B_{as}(t') \\
& + R_{as}(t)B_{as}(t')\rho_{s_B}(t)R_{sa}(t')B_{sa}(t')] + Adj.
\end{aligned} \quad (A.5)$$

where $B_{ee}(t) = A_1(t) + A_2(t)$, $B_{ss}(t) = \beta^2 A_1(t) + \alpha^2 A_2(t)$, $B_{aa} = \alpha^2 A_1(t) + \beta^2 A_2(t)$, $B_{sa}(t) = \alpha\beta [A_1(t) - A_2(t)]$, and $B_{as}(t) = B_{sa}^*(t)$.

The structure of integrals appearing in Eq. (A.5) are of the type

$$Tr_B \int_0^t dt' \rho_{s_B}(t) B_{jk}(t) B_{lm}(t') \rho(t) \quad (j, k, l, m) = e, s, a \quad (A.6)$$

For example,

$$\begin{aligned}
& Tr_B \int_0^t dt' \rho_{s_B}(t) B_{ee}(t) B_{ee}(t') \rho_{s_B}(t) \\
& = Tr_B \int_0^t dt' \rho_{s_B}(t) \left[\sum_{q_j} \lambda_{q_j} \left(b_{q_j}^+ e^{i\omega_{L'} t'} + b_{q_j} e^{-i\omega_{L'} t'} \right) \right. \\
& \quad \times \sum_{q'_j} \lambda_{q'_j} \left(b_{q'_j}^+ e^{i\omega_{L'} t'} + b_{q'_j} e^{-i\omega_{L'} t'} \right) \Big] \\
& = \rho(t) \int_0^t dt' \sum_{q_j} \lambda_{q_j}^2 \langle b_{q_j}^+ b_{q_j} \rangle e^{i\omega_{L'}(t-t')} + \hbar^2 \int_0^t dt' \sum_{q_j} \lambda_{q_j}^2 \langle b_{q_j} b_{q_j}^+ \rangle e^{-i\omega_{L'}(t-t')} \\
& = \rho_s(t) \sum_{q_1} \lambda_{q_1}^2 \langle b_{q_1}^+ b_{q_1} \rangle \pi \delta(\omega_{q_1}) + \rho_s(t) \sum_{q_2} \lambda_{q_2}^2 \langle b_{q_2} b_{q_2}^+ \rangle \pi \delta(\omega_{q_2})
\end{aligned} \quad (A.7)$$

where $\rho_s(t)$ is the matrix density of the atomic system. In the above calculations the hypothesis of independent reservoirs that we have made consists in assuming that $\langle b_{q_l} b_{q_m}^+ \rangle = 0$ ($l \neq m$). Taking into account the statistical properties of the phonon baths given in Eq. (28), we obtain

$$\begin{aligned}
& Tr_B \int_0^t dt' \rho_{s_B}(t) B_{ee}(t) B_{ee}(t') \\
& = \pi \rho_s(t) \sum_{q_1} \lambda_{q_1}^2 (\omega_{q_1}) (n_1(\omega_{q_1}) + 1) + \pi \rho_s(t) \sum_{q_2} \lambda_{q_2}^2 (\omega_{q_1}) (n_2(\omega_{q_2})) \\
& = \hbar^2 \rho(t) [(n_1(\omega_{q_1}) + 1) + n_1(\omega_{q_1})] \Gamma_{pn}
\end{aligned} \quad (A.8)$$

where $\Gamma_{pn} = \sum_{j=1,2} \sum_{q_j} \left(\frac{\lambda_{q_j}}{\hbar} \right)^2 \delta(\omega_{q_j} - 2J_{eff})$ is the dissipation rate induced by the electron-phonon environment. The other terms appearing in Eq. (A.5) can be obtained in similar procedure. It is straightforward to obtain the Eqs. (30)–(31) of the current paper.

Appendix B. Appendix density matrix equations

From Eqs. (18), we obtain the equations of evolution for the elements of the density matrix in the Dicke basis:

$$\begin{aligned}
\dot{\rho}_{ee}(t) &= -2(\Gamma_s + \Gamma_a) \rho_{ee} - i(\beta\Omega_2 - \alpha\Omega_1)(\rho_{se} - \rho_{es}) \\
&\quad - i(\alpha\Omega_2 - \beta\Omega_1)(\rho_{ae} - \rho_{ea}), \\
\dot{\rho}_{ss}(t) &= -2(\Gamma_s + F_{sa}) \rho_{ss} + 2\Gamma_s \rho_{ee} - \Gamma_{as}(\rho_{as} + \rho_{sa}) \\
&\quad + i(\beta\Omega_2 + \alpha\Omega_1)(\rho_{se} - \rho_{es}) + i(\alpha\Omega_2 + \beta\Omega_1)(\rho_{sg} - \rho_{gs}), \\
\dot{\rho}_{aa}(t) &= -2(\Gamma_a + F_{as}) \rho_{aa} + 2F_{sa} \rho_{ss} + 2\Gamma_a \rho_{ee} - \Gamma_{as}(\rho_{as} + \rho_{sa}) \\
&\quad + i(\beta\Omega_2 - \alpha\Omega_1)(\rho_{ga} - \rho_{ag}) + i(\alpha\Omega_2 - \beta\Omega_1)(\rho_{ae} - \rho_{ea}) \\
&\quad + i\Omega_2 [\beta(\rho_{ae} + \rho_{gs}) + \alpha(\rho_{ag} - \rho_{es})]
\end{aligned} \quad (B.1)$$

and the coherences,

$$\begin{aligned}
\dot{\rho}_{as}(t) &= -[F_a + F_s + F_{sa} + F_{sa} - 2X_{sa} - i(\lambda_2 - \lambda_3)] \rho_{as} \\
&\quad - (\Gamma_s + \Gamma_a) \rho_{as} - \Gamma_{as}(\rho_{ss} + \rho_{aa} - 2\rho_{ee}) \\
&\quad + i\Omega_2 [\beta(\rho_{ae} + \rho_{gs}) + \alpha(\rho_{ag} - \rho_{es})] - i\Omega_1 [\alpha(\rho_{gs} - \rho_{ae}) - \beta(\rho_{es} + \rho_{ag})] \\
\dot{\rho}_{ga}(t) &= -[(F_a + \Gamma_a + F_{as}) - i(\lambda_3 - \lambda_4)] \rho_{ga} - \Gamma_{as} \rho_{gs} \\
&\quad - (\alpha^2 - \beta^2) \Gamma_a \rho_{se} + (2\alpha\beta\Gamma - \Gamma_{12}) \rho_{ae} \Gamma_a \rho_{as} - \Gamma_{as}(\rho_{ss} + \rho_{aa} - 2\rho_{ee}) \\
&\quad + i\Omega_2 [\beta(\rho_{aa} - \rho_{gg}) + \alpha(\rho_{ge} - \rho_{sa})] - i\Omega_1 [\beta(\rho_{sa} + \rho_{ge}) + \alpha(\rho_{aa} - \rho_{gg})], \\
\dot{\rho}_{ge}(t) &= -[\Gamma_s + \Gamma_a - i(\lambda_1 - \lambda_4)] \rho_{ge} \\
&\quad + i\Omega_2 [\beta(\rho_{ae} + \rho_{gs}) - \alpha(\rho_{se} - \rho_{ga})] - i\Omega_1 [\beta(\rho_{se} + \rho_{ga}) + \alpha(\rho_{ae} - \rho_{gs})], \\
\dot{\rho}_{gs}(t) &= -[(\Gamma_s + F_{sa}) - i(\lambda_2 - \lambda_4)] \rho_{gs} - \Gamma_{as} \rho_{gs} \\
&\quad - (\alpha^2 - \beta^2) \Gamma_a \rho_{ae} + (2\alpha\beta\Gamma + \Gamma_{12}) \rho_{se} \\
&\quad + i\Omega_2 [\alpha(\rho_{gg} - \rho_{ss}) + \beta(\rho_{as} + \rho_{ge})] - i\Omega_1 [\beta(\rho_{ss} - \rho_{gg}) + \alpha(\rho_{as} - \rho_{ge})], \\
\dot{\rho}_{ae}(t) &= -[F_a + F_e + F_{as} + \Gamma_s - 2X_{ea} + 2\Gamma_a - i(\lambda_1 - \lambda_3)] \rho_{ae} \\
&\quad + i\Omega_2 [\beta(\rho_{as} + \rho_{ge}) + \alpha(\rho_{aa} - \rho_{ee})] - i\Omega_1 [\alpha(\rho_{ge} - \rho_{as}) + \beta(\rho_{aa} - \rho_{ee})], \\
\dot{\rho}_{se}(t) &= -[F_s + F_e + F_{sa} + \Gamma_a - 2X_{ea} + 2\Gamma_s - i(\lambda_1 - \lambda_2)] \rho_{se} \\
&\quad + i\Omega_2 [\beta(\rho_{ss} - \rho_{ee}) + \alpha(\rho_{sa} - \rho_{ge})] - i\Omega_1 [\alpha(\rho_{ee} - \rho_{ss}) + \beta(\rho_{ge} + \rho_{sa})],
\end{aligned} \quad (B.2)$$

with $\rho_{gg}(t) + \rho_{ee}(t) + \rho_{ss}(t) + \rho_{aa}(t) = 1$ and $\rho_{nm}(t) = \rho_{mn}^*(t)$.

References

- [1] J.I. Cirac, P. Zoller, Quantum computations with cold trapped ions, *Phys. Rev. Lett.* 74 (1995) 4091, <http://dx.doi.org/10.1103/PhysRevLett.74.4091>.
- [2] C. Bennett, D. DiVincenzo, Quantum information and computation, *Nature* 404 (2000) 247, <http://dx.doi.org/10.1038/35005001>.
- [3] H.P. Breuer, F. Petruccione, *Quantum Computation and Quantum Information*, Cambridge University Press, Cambridge, 2000.
- [4] P. Kok, W.J. Munro, K. Nemoto, T.C. Ralph, J.P. Dowling, G.J. Milburn, Linear optical quantum computing with photonic qubits, *Rev. Modern Phys.* 79 (2007) 135, <http://dx.doi.org/10.1103/RevModPhys.79.135>.
- [5] G.J. Milburn, Photons as qubits, *Phys. Scr.* T137 (2009) 014003, <http://dx.doi.org/10.1088/0031-8949/2009/T137/014003>.
- [6] I. Gonzalo, M.A. Antón, Entangling non planar molecules via inversion doublet transition with negligible spontaneous emission, *Phys. Chem. Chem. Phys.* 20 (2019) 10523, <http://dx.doi.org/10.1039/C8CP07764A>.
- [7] I. Bloch, Quantum coherence and entanglement with ultracold atoms in optical lattices, *Nature* 453 (2008) 1016, <http://dx.doi.org/10.1038/nature07126>.
- [8] M.D. Lukin, Trapping and manipulating photon states in atomic ensembles, *Rev. Modern Phys.* 75 (2003) 457, <http://dx.doi.org/10.1103/RevModPhys.75.457>.
- [9] R. Blatt, D. Wineland, Entangled states of trapped atomic ions, *Nature* 453 (2008) 1008, <http://dx.doi.org/10.1038/nature07125>.
- [10] A.I. Y. Yamamoto, *Mesoscopic Quantum Optics*, Wiley-Interscience, New York, 2001.
- [11] C. Dory, K.A. Fischer, K. Muller, K.G. Lagoudakis, T. Sarmiento, A. Rundquist, J.L. Zhang, Y. Kelaita, J. Vuckovic, Complete coherent control of a quantum dot strongly coupled to a nanocavity, *Sci. Rep.* 6 (1) (2016) 1, <http://dx.doi.org/10.1038/srep25172>.
- [12] A. Majumdar, M. Bajcsy, A. Rundquist, E. Kim, J. Vuckovic, Phonon-mediated coupling between quantum dots through an off-resonant microcavity, *Phys. Rev. B* 85 (2016) 195301, <http://dx.doi.org/10.1103/PhysRevB.85.195301>.
- [13] I. Wilson-Rae, I.A. Imamoglu, Quantum dot cavity-QED in the presence of strong electron-phonon interactions, *Phys. Rev. B* 65 (2002) 235311, <http://dx.doi.org/10.1103/PhysRevB.65.235311>.
- [14] M.A. Antón, I. Gonzalo, F. Carreño, Bichromatically-controlled entanglement between asymmetric quantum dots in a photonic cavity, *J. Phys. B: At. Mol. Opt. Phys.* 54 (2020) 015504, <http://dx.doi.org/10.1088/1361-6455/abc9ca>.
- [15] A. Galiatdinov, A.N. Korotkov, J.M. Martinis, Resonator-zero-qubit architecture for superconducting qubits, *Phys. Rev. A* 85 (2012) 042321, <http://dx.doi.org/10.1103/PhysRevA.85.042321>.
- [16] R. Harris, A.J. Berkley, M.W. Johnson, P. Bunyk, S. Govorkov, M.C. Thom, S. Uchaikin, A.B. Wilson, E.H. J. Chung, J.D. Biamonte, A.Y. Smirnov, M.H.S. Amin, A.M. van den Brink, Sign and magnitude-tunable coupler for superconducting flux qubits, *Phys. Rev. Lett.* 98 (2007) 177001, <http://dx.doi.org/10.1103/PhysRevLett.98.177001>.
- [17] M.B. Plenio, P.L. Knight, The quantum-jump approach to dissipative dynamics in quantum optics, *Rev. Modern Phys.* 70 (1998) 101, <http://dx.doi.org/10.1103/RevModPhys.70.101>.
- [18] J. Paz, W. Zurek, Environment-induced decoherence and the transition from quantum to classical, in: *Lecture Notes in Physics*, vol. 70, Springer-Verlag, Berlin, 2002, p. 77.

- [19] M.J. Kastoryano, F. Reiter, A.S. Sørensen, Dissipative preparation of entanglement in optical cavities, *Phys. Rev. Lett.* 106 (2011) 090502, <http://dx.doi.org/10.1103/PhysRevLett.106.090502>.
- [20] C. Marr, A. Beige, G. Rempe, Entangled-state preparation via dissipation-assisted adiabatic passages, *Phys. Rev. A* 68 (2003) 033817, <http://dx.doi.org/10.1103/PhysRevA.68.033817>.
- [21] Z. Man, Y. Xia, R.L. Franco, Cavity-based architecture to preserve quantum coherence and entanglement, *Sci. Rep.* 5 (2015) 13843, <http://dx.doi.org/10.1038/srep13843>.
- [22] J. Majer, J.M. Chow, J.M. Gambetta, J. Koch, B.R. Johnson, J.A. Schreier, L. Frunzio, D.I. Schuster, A.A. Houck, A. Wallraff, A. Blais, M.H. Devoret, S.M. Girvin, R.J. Schoelkopf, Coupling superconducting qubits via a cavity bus, *Nature* 449 (2007) 443, <http://dx.doi.org/10.1038/nature06184>.
- [23] S. Clark, A. Parkins, Entanglement and entropy engineering of atomic two-qubit states, *Phys. Rev. Lett.* 90 (2003) 047905, <http://dx.doi.org/10.1103/PhysRevLett.90.047905>.
- [24] L. Duan, H. Kimble, Efficient engineering of multiatom entanglement through single-photon detections, *Phys. Rev. Lett.* 90 (2003) 253601, <http://dx.doi.org/10.1103/PhysRevLett.90.253601>.
- [25] S. Maier, *Plasmonics: Fundamentals and Applications*, Springer, Berlin, Berlin, 2007.
- [26] V. Yannopapas, E. Paspalakis, N. Vitanov, Plasmon-induced enhancement of quantum interference near metallic nanostructures, *Phys. Rev. Lett.* 103 (6) (2006) 063602, <http://dx.doi.org/10.1103/PhysRevLett.103.063602>.
- [27] Y. Vladimirova, V. Klimov, V. Pastukhov, V. Zadkov, Resonance fluorescence of a two-level quantum emitter near a plasmonic nanoparticle: role of the near-field polarization, *Phys. Rev. A* 85 (5) (2012) 053408, <http://dx.doi.org/10.1088/1555-6611/aa5240>.
- [28] F. Carreño, M. Antón, V. Yannopapas, E. Paspalakis, Control of resonance fluorescence of a four-level quantum emitter near a plasmonic nanostructure, *Phys. Rev. A* 95 (4) (2017) 043825, <http://dx.doi.org/10.1103/PhysRevA.95.043825>.
- [29] N. Iliopoulos, A.F. Terzis, V. Yannopapas, E. Paspalakis, Two-qubit correlations via a periodic plasmonic nanostructure, *Ann. Physics* 365 (4) (2016) 38, <http://dx.doi.org/10.1016/j.aop.2015.10.022>.
- [30] J. Hou, K. Slowik, F. Lederer, C. Rockstuhl, Dissipation-driven entanglement between qubits mediated by plasmonic nanoantennas, *Phys. Rev. B* 89 (4) (2014) 235413, <http://dx.doi.org/10.1103/PhysRevB.89.235413>.
- [31] F. Zhang, D. Zhao, Y. Gu, H. Chen, X. Hu, Q. Gong, Detuning-determined qubit-qubit entanglement mediated by plasmons: An effective model for dissipative systems, *J. Appl. Phys.* 121 (2017) 203105, <http://dx.doi.org/10.1063/1.4984206>.
- [32] S. Nicolosi, A. Napoli, A. Messina, F. Petruccione, Dissipation-induced stationary entanglement in dipole-dipole interacting atomic samples, *Phys. Rev. A* 70 (2004) 022511, <http://dx.doi.org/10.1103/PhysRevA.70.022511>.
- [33] A. Gonzalez-Tudela, D. Martin-Cano, E. Moreno, L. Martin-Moreno, C. Tejedor, F.J. Garcia-Vidal, Entanglement of two qubits mediated by one-dimensional plasmonic waveguides, *Phys. Rev. Lett.* 106 (2011) 020501, <http://dx.doi.org/10.1103/PhysRevLett.106.020501>.
- [34] A. Martin-Cano, L. Gonzalez-Tudela, F. Martin-Moreno, C. Garcia-Vidal, C. Tejedor, E. Moreno, Dissipation-driven generation of two-qubit entanglement mediated by plasmonic waveguides, *Phys. Rev. B* 84 (2011) 235306, <http://dx.doi.org/10.1103/PhysRevB.84.235306>.
- [35] A.H. Gangaraj, A. Nemilentsau, G.W. Hanson, S. Hughes, Transient and steady-state entanglement mediated by three-dimensional plasmonic waveguides, *Opt. Express* 23 (2015) 22330, <http://dx.doi.org/10.1364/OE.23.22330>.
- [36] G.Y. Chen, Y. Chen, Generating maximum entanglement under asymmetric couplings to surface plasmons, *Opt. Lett.* 37 (2012) 1337, <http://dx.doi.org/10.1364/OL.37.001337>.
- [37] A.J. Ramsay, A.V. Gopal, E.M. Gauger, A. Nazir, B. Lovett, A.M. Fox, M.S. Skolnick, Damping of exciton Rabi rotations by acoustic phonons in optically excited InGaAs/GaAs quantum dots, *Phys. Rev. Lett.* 104 (2010) 017402, <http://dx.doi.org/10.1103/PhysRevLett.104.017402>.
- [38] D. Christiansen, M. Selig, G. Berghäuser, R. Schmidt, I. Niehues, R. Schneider, A. Arora, S.M. de Vasconcellos, R. Bratschitsch, E. Malic, A. Knorr, Phonon sidebands in monolayer transition metal dichalcogenides, *Phys. Rev. Lett.* 119 (2011) 16042, <http://dx.doi.org/10.1103/PhysRevLett.119.16042>.
- [39] M.M. Glazov, Phonon wind and drag of excitons in monolayer semiconductors, *Phys. Rev. B* 100 (2019) 16042, <http://dx.doi.org/10.1103/PhysRevB.100.045426>.
- [40] A. Nazir, D.P.S. McCutcheon, Modelling exciton-phonon interactions in optically driven quantum dots, *J. Phys.: Condens. Matter* 28 (2016) 103002, <http://dx.doi.org/10.1088/0953-8984/28/10/103002>.
- [41] C. Roy, S. Hughes, Influence of electron-acoustic-phonon scattering on intensity power broadening in a coherently driven quantum-dot-cavity system, *Phys. Rev. X* 1 (2011) 021009, <http://dx.doi.org/10.1103/PhysRevX.1.021009>.
- [42] E.D.K. A. Majumdar and, Y. Gong, M. Bajcsy, M. Vučković, Phonon mediated off-resonant quantum dot-cavity coupling under resonant excitation of the quantum dot, *Phys. Rev. B* 84 (2011) 16042, <http://dx.doi.org/10.1103/PhysRevB.84.085309>.
- [43] M. Plenio, S. Huelga, Entangled light from white noise, *Phys. Rev. Lett.* 88 (2002) 197901, <http://dx.doi.org/10.1103/PhysRevLett.88.197901>.
- [44] J. Xu, S. Li, Control of the entanglement of two atoms in an optical cavity via white noise, *New J. Phys.* 7 (2005) 72, <http://dx.doi.org/10.1088/1367-2630/7/1/072>.
- [45] A.O. Caldeira, A.J. Leggett, Quantum tunnelling in a dissipative system, *Ann. Physics* 149 (1983) 374, [http://dx.doi.org/10.1016/0003-4916\(83\)90202-6](http://dx.doi.org/10.1016/0003-4916(83)90202-6).
- [46] D. Braun, Creation of entanglement by interaction with a common heat bath, *Phys. Rev. Lett.* 89 (2002) 277901, <http://dx.doi.org/10.1103/PhysRevLett.89.277901>.
- [47] J.-Q. Liao, J.-F. Huang, L.-M. Kuang, C.P. Sun, Coherent excitation-energy transfer and quantum entanglement in a dimer, *Phys. Rev. A* 82 (2010) 052109, <http://dx.doi.org/10.1103/PhysRevA.82.052109>.
- [48] P.J. Dodd, J.J. Halliwell, Disentanglement and decoherence by open system dynamics, *Phys. Rev. A* 69 (2004) 052105, <http://dx.doi.org/10.1103/PhysRevA.69.052105>.
- [49] O. Cotlet, B.W. Lovett, Probing bath-induced entanglement in a qubit pair by measuring photon correlations, *New J. Phys.* 16 (2014) 103016, <http://dx.doi.org/10.1088/1367-2630/16/10/103016>.
- [50] L.D. Contreras-Pulido, R. Aguado, Entanglement between charge qubits induced by a common dissipative environment, *Phys. Rev. B* 77 (2008) 155420, <http://dx.doi.org/10.1103/PhysRevB.77.155420>.
- [51] E. Cecoi, V. Ciornea, A. Isar, M. Macovei, Entanglement of a laser-driven pair of two-level qubits via its phonon environment, *J. Opt. Soc. Amer. B* 35 (2018) 1127, <http://dx.doi.org/10.1364/JOSAB.35.001127>.
- [52] R. Manson, K. Roy-Choudhury, S. Hughes, Polariton master equation theory of pulse-driven phonon-assisted population inversion and single-photon emission from quantum-dot excitons, *Phys. Rev. B* 93 (2016) 155423, <http://dx.doi.org/10.1103/PhysRevB.93.155423>.
- [53] S. Lüker, T. Kuhn, D.E. Reiter, Phonon-assisted dark exciton preparation in a quantum dot, *Phys. Rev. B* 95 (2017) 195305, <http://dx.doi.org/10.1103/PhysRevB.95.195305>.
- [54] E. Rozbicki, P. Machnikowsky, Quantum kinetic theory of phonon-assisted excitation transfer in quantum dot molecules, *Phys. Rev. Lett.* 100 (2008) 027401, <http://dx.doi.org/10.1103/PhysRevLett.100.027401>.
- [55] P. Johnson, R. Christy, Optical constants of the noble metals, *Phys. Rev. B* 6 (1972) 4370, <http://dx.doi.org/10.1103/PhysRevB.6.4370>.
- [56] Y.B. Gao, C.P. Sun, Factorization of the dephasing process in a quantum open system, *Phys. Rev. E* 75 (2007) 011105, <http://dx.doi.org/10.1103/PhysRevE.75.011105>.
- [57] A. Ridolfo, O.D. Stefano, N. Fina, R. Saija, S. Savasta, Quantum plasmonics with quantum dot-metal nanoparticle molecules: Influence of the Fano effect on photon statistics, *Phys. Rev. Lett.* 105 (2010) 263601, <http://dx.doi.org/10.1103/PhysRevLett.105.263601>.
- [58] M.O. Scully, M.S. Zubairy, *Quantum Optics*, Oxford University Press, Cambridge University Press, 1997.
- [59] W. Zhang, A.O. Govorov, G.W. Bryant, Semiconductor-metal nanoparticle molecules: Hybrid excitons and the nonlinear Fano effect, *Phys. Rev. Lett.* 97 (2006) 146804, <http://dx.doi.org/10.1103/PhysRevLett.97.146804>.
- [60] H.P. Breuer, F. Petruccione, *The Theory of Open Quantum Systems*, Oxford University Press, Oxford, 2002.
- [61] A. Leggett, S. Chakravarty, A. Dorsey, M. Fisher, A. Garg, Zwerger, Dynamics of the dissipative two-state system, *Rev. Modern Phys.* 59 (1987) 1, <http://dx.doi.org/10.1103/RevModPhys.59.1>.
- [62] Z. Ficek, R. Tanas, Entangled states and collective nonclassical effects in two-atom systems, *Phys. Rep.* 372 (2002) 369, [http://dx.doi.org/10.1016/S0370-1573\(02\)00368-X](http://dx.doi.org/10.1016/S0370-1573(02)00368-X).
- [63] D. Zhao, Y. Gu, H. Chen, J. Ren, T. Zhang, Q. Gong, Quantum statistics control with a plasmonic nanocavity: Multimode-enhanced interferences, *Phys. Rev. A* 92 (2015) 033836, <http://dx.doi.org/10.1103/PhysRevA.92.033836>.
- [64] T. Takagahara, Theory of exciton dephasing in semiconductor quantum dots, *Phys. Rev. B* 60 (1999) 2638, <http://dx.doi.org/10.1103/PhysRevB.60.2638>.
- [65] S. Ulrich, S. Ates, S. Reitzenstein, A. Löffler, A. Forchel, P. Michler, Dephasing of triplet-sideband optical emission of a resonantly driven InAs/GaAs quantum dot inside a microcavity, *Phys. Rev. Lett.* 106 (2011) 247402, <http://dx.doi.org/10.1103/PhysRevLett.106.247402>.
- [66] B. Krummheuer, V.M. Axt, T. Kuhn, Theory of pure dephasing and the resulting absorption line shape in semiconductor quantum dots, *Phys. Rev. B* 65 (2002) 247402, <http://dx.doi.org/10.1103/PhysRevB.65.195313>.
- [67] A.J. Ramsay, T.M. Godden, J. Boyle, E.M. Gauger, A. Nazir, B. Lovett, Phonon-induced Rabi-frequency renormalization of optically driven single InGaAs/GaAs quantum dots, *Phys. Rev. Lett.* 105 (2010) 177402, <http://dx.doi.org/10.1103/PhysRevLett.105.177402>.
- [68] D.P.S. McCutcheon, A. Nazir, Quantum dot Rabi rotations beyond the weak exciton-phonon coupling regime, *New J. Phys.* 12 (2010) 113042, <http://dx.doi.org/10.1088/1367-2630/12/11/113042>.

- [69] W.K. Wothers, Entanglement of formation of an arbitrary state of two qubits, *Phys. Rev. Lett.* 80 (1998) 2245, <http://dx.doi.org/10.1103/PhysRevLett.80.2245>.
- [70] G. Chen, N.H. Bonadeo, D.G. Steel, D. Gammon, D.S. Katzer, D. Park, L.J. Sham, Optically induced entanglement of excitons in a single quantum dot, *Science* 289 (2000) 1906, <http://dx.doi.org/10.1126/science.289.5486.1906>.
- [71] A. Hichri, S. Jaziri, R. Ferreira, Entangled bell states of two electrons in coupled quantum dots—phonon decoherence, *Phys. Status Solidi C* 1 289 (2004) 598, <http://dx.doi.org/10.1016/j.physe.2004.04.036>.
- [72] R.G. Unanyan, B.W. Shore, K. Bergmann, Entangled-state preparation using adiabatic population transfer, *Phys. Rev. A* 63 (2001) 043405, <http://dx.doi.org/10.1103/PhysRevA.63.043405>.
- [73] V.S. Malinovsky, I.R. Sola, Quantum control of entanglement by phase manipulation of time-delayed pulse sequences. I, *Phys. Rev. A* 70 (2004) 042304, <http://dx.doi.org/10.1103/PhysRevA.70.042304>.
- [74] Z. Ficek, R. Tanas, Entangled states and collective nonclassical effects in two-atom systems, *Phys. Rep.* 372 (2002) 369, [http://dx.doi.org/10.1016/S0370-1573\(02\)00368-X](http://dx.doi.org/10.1016/S0370-1573(02)00368-X).
- [75] C. Creatore, R.T. Brierley, R.T. Phillips, P.B. Littlewood, P.R. Eastham, Creation of entangled states in coupled quantum dots via adiabatic rapid passage, *Phys. Rev. B* 86 (2012) 155442, <http://dx.doi.org/10.1103/PhysRevB.86.155442>.
- [76] Y. Guo, X. Luo, S. Ma, C.-C. Shu, All-optical generation of quantum entangled states with strictly constrained ultrafast laser pulses rapid passage, *Phys. Rev. A* 100 (2019) 023409, <http://dx.doi.org/10.1103/PhysRevA.100.023409>.
- [77] Z. Ficek, R. Tanas, Delayed sudden birth of entanglement, *Phys. Rev. A* 77 (2008) 054301, <http://dx.doi.org/10.1103/PhysRevA.77.054301>.
- [78] H. Kim, D. Sridharan, T.C. Shen, G.S. Solomon, E. Waks, Strong coupling between two quantum dots and a photonic crystal cavity using magnetic field tuning, *Opt. Express* 19 (2011) 2589, <http://dx.doi.org/10.1364/OE.19.002589>.